

OF-VO: Reliable Navigation among Pedestrians Using Commodity Sensors

Jing Liang¹, Yi-Ling Qiao¹ and Dinesh Manocha

Abstract—We present a novel algorithm for safe navigation of a mobile robot among pedestrians. Our approach uses commodity visual sensors, including RGB-D cameras and a 2D lidar, for explicitly predicting the velocities and positions of surrounding obstacles through optical flow estimation and object detection. Given these partial observations of the environment, we present a modified velocity-obstacle (VO) algorithm to compute collision-free trajectories for the robot. A key aspect of our work is the coupling between the perception (OF: optical flow) and planning (VO) components for reliable navigation. Overall, our OF-VO algorithm is a hybrid combination of learning-based and model-based methods and offers better performance over prior algorithms in terms of navigation time and success rate of collision avoidance. We highlight the realtime performance of OF-VO in simulated and real-world dynamic scenes on a Turtlebot robot navigating among pedestrians with commodity sensors. A demo video is available at <https://youtu.be/1brBIZRaxBs>

I. INTRODUCTION

Mobile robots are currently deployed in a wide range of scenarios including warehouses, airports, malls, and offices. In these indoor and outdoor spaces, robots are used to perform routine tasks such as delivering goods and guiding customers. A key issue is to perform reliable navigation in terms of avoiding collisions with pedestrians and other obstacles.

There are extensive works on robot navigation and collision-avoidance in dynamic scenes. These include model-based techniques based on velocity obstacles, sampling-based algorithms, optimization methods, etc. However, most of them assume an exact representation of the environment. Many extensions have been proposed for real-world scenes using vector-field-based approaches [1], [31], which only work well for static obstacles. Other techniques have been proposed for dynamic scenes [12], [11], [20], [16], but their performance may vary in different environments [21]. Furthermore, many of them rely on expensive sensors like rangefinders or 3D lidars.

Recently, a number of learning-based approaches are proposed to perform robot navigation and collision avoidance [9], [44], [10], [42], [29], [34], [8], [43]. These algorithms can reliably handle sensor noise in many cases and tend to recover the expert policy in many scenarios. However, it is challenging to predict their performance in new or unknown scenes. This is due to the fact that training a policy with a neural network is almost like a ‘black box’, with little guarantees on its performance. Overall, we need better techniques for explainability and interpretability of learning-based navigation algorithms.

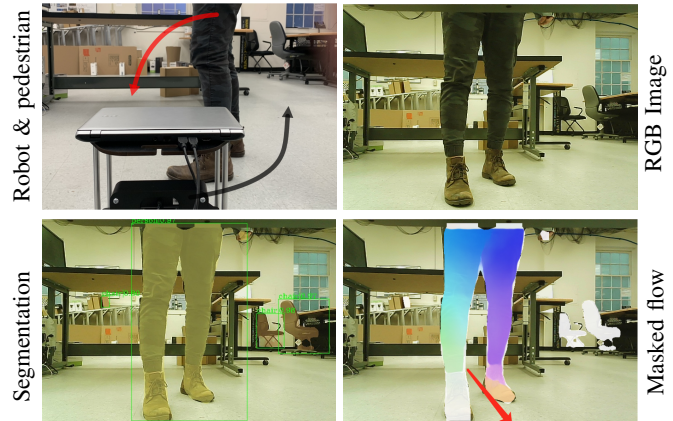


Fig. 1. Navigation among pedestrian in an indoor scene. We highlight the scene captured using a commodity camera mounted on the robot (top) the red and black curved arrows represent the trajectories of the pedestrian and the robot, respectively. The bottom row highlights the segmentation and optical flow using our OF-VO algorithm, which are used for collision-free trajectory computation. The red straight arrow shows the velocity of the pedestrian computed by our algorithm.

Main Results: We present a novel hybrid scheme for safe navigation of a mobile robot among pedestrians and other obstacles. Our approach take advantage of learning-based module to handle sensor data and model-based module to compute safe velocities for collision avoidance. Instead of developing an end-to-end approach, we use separate components for perception and planning. The novel components of our work include:

- Detecting static and dynamic obstacles using mask R-CNN and estimate their positions and velocities using optical flows.
- We present a modified velocity obstacle algorithm that uses partial observations corresponding to optical flows as inputs and computes a collision-free trajectory for the robot.
- We present a real-world navigation scheme (OF-VO) that uses commodity sensors corresponding to RGB-D cameras and 2D lidars that can be easily mounted on mobile robots.

We have tested our algorithm on a Turtlebot robot with cheap commodity sensors including an RGB-D camera, Orbecc Astra (around 100\$), and a 2-D Lidar, Hokuyo (around 1000\$). We have evaluated OF-VO in simulated and real-world environments with multiple pedestrians, including high-density environments with more than 10 pedestrians

in a $5 \times 5m^2$ scenario. We have also compared with prior model-based methods like DWA [12] and deep-reinforcement learning algorithms like [9], and achieve at most 2 – 5X improvement in success rate (and reliability) and around 40% reduction in the navigation time in complex scenarios.

II. BACKGROUND AND RELATED WORK

In this section, we briefly survey related work on local navigation and collision avoidance. We also give an overview of prior work in computer vision on object segmentation and motion detection.

A. Collision Avoidance

With recent progress in machine learning, many researchers have been using learning algorithms to train policies for robot collision avoidance. [2], [10] use POMDP to navigate robots in uncertain scenarios. [25] uses deep learning to train an end-to-end network in indoor scenarios. This method has shown good performance in avoiding static obstacles, but may not give good results for dynamic obstacles. [4], [34] uses imitation learning, GAIL or modified Dagger, to train policies with performances similar to those of expert strategies. Those approaches can be used in dynamic scenarios, but they require expert policies to imitate.

With the development of reinforcement learning, policies are also being trained with different sensors in different scenarios. Cameras are widely used as inputs to reinforcement learning algorithms. [42] uses deep double-Q learning with RGB cameras to train policy in cluttered scenarios, [24] uses the A3C algorithm, and [44] uses the Target-final algorithm to train policies based on RGB images in indoor scenarios. [9] use lidar along PPO algorithm [30] to navigate multiple robots in scenarios with static and dynamic obstacles. However, it is hard to provide any reliability guarantees for these methods.

Many algorithms for dynamic algorithms have been proposed based on velocity obstacles (VO) [11] and its extensions [20], [37], [14]. They can also handle dynamics constraints corresponding to linear dynamics [3], acceleration constraints [38], car-like robots [40], as well as sensing uncertainty [14], [39]. We use an extension of [32] with distance prediction to handle differential drive robots.

B. Motion Estimation

Estimating the positions and velocities of moving objects plays an important role in our navigation algorithm. Many previous works [23], [17], [29] estimate velocities through trajectory tracking and prediction. However, tracking algorithms may not perform consistently well in dense scenes. They may lose tracking targets and may result in inaccurate position and velocity estimations. Instead, we break down the motion perception into two independent stages, optical flow estimation, and object detection.

Optical flow (OF) is the displacement of the pixel position between two consecutive images. Sparse OF only computes the flow on some landmark points, which takes less time. For real-time performance, some methods [36], [45], [6] use

sparse OF to avoid collisions. Their basic idea is that pixels of closer objects tend to move faster, such that the robot steers to the side with smaller optical flow. Although this rule seems direct and intuitive, the underlying assumption is over-simplified and may not hold in complex dynamics scenes. Traditional dense optical flow estimation is achieved by optimization [18], [5] with smoothness constraints, which takes several minutes to compute one image pair. Recently, some learning-based methods based on neural networks [7], [19], [33] estimate the optical flow with accuracy comparable to traditional methods but run orders of magnitude faster. In our method, we use FlowNet2 [19] to estimate the motion between two frames.

State-of-the-art detection methods like [13], [28] can detect different categories of objects and present their bounding boxes. These learning-based methods can predict with high efficiency and accuracy. In order to estimate the motion with dense optical flows, we need to segment the objects from the background. Mask-RCNN [15] and YOLO [26], [27] are able to provide pixel-level segmentation of different objects.

III. OVERVIEW

TABLE I. Notation and symbols used in our approach.

Notation	Defination
\mathbf{I}	Image captured from the RGB camera
\mathbf{D}	Depth map captured from the depth camera
\mathbf{O}	Optical flow estimation
\mathbf{M}_i	Segmentation mask of the i_{th} obstacle
$\mathbf{v}_r, \mathbf{v}_o$	Velocity of the robot and obstacles
$\mathbf{p}_r, \mathbf{p}_o$	Position of the robots or obstacles
\mathbf{v}_{pref}	Preferred velocity of robot
\mathbf{v}_{out}	The output velocity from our method
\mathbf{v}_{vo}	The output of OF-VO before using dynamic constraint
$V_{r o}^T$	Veclocity obstacle of robot r caused by obstacle o in step-time T
V_r^T	Total available velocity set
V_a	Allowed velocity space
V_c	Velocity space under constraints of partial observation
c_x, c_y, f_x, f_y	Principal point and focal lengths
t_0, t_1	Time stamp of the last and current frames
T	time step
r_r, r_o	radius of robot and obstacle
s_i, s_r	shape of i_{th} obstacle or robot

Our approach is designed for non-holonomic robots that can be driven by linear and angular velocity. During each timestep, the robot knows the relative position of its target/goal and needs to navigate to the target in an environment with both static and dynamic obstacles. Each obstacle has a velocity \mathbf{v}_i at position \mathbf{p}_i . On the way to the goal, the robot can perceive surrounding obstacles by using a 2D Lidar and RGB-D camera and avoid potential collisions. Figure 2 shows the pipeline of our approach, OFVO. Notations and symbols are summarized in Table I.

At each timestep, the robot receives two consecutive RGB-D and Lidar frames to calculate the instantaneous velocities of the surrounding obstacles. Assume that the current time is t_1 and its previous time step is $t_0 < t_1$. From the RGB-D camera we have two pairs of RGB images $\mathbf{I}_{t_1}, \mathbf{I}_{t_0} \in \mathbb{R}^{h \times w \times 3}$ and depth images $\mathbf{D}_{t_1}, \mathbf{D}_{t_0} \in \mathbb{R}^{h \times w}$, where h, w is the height

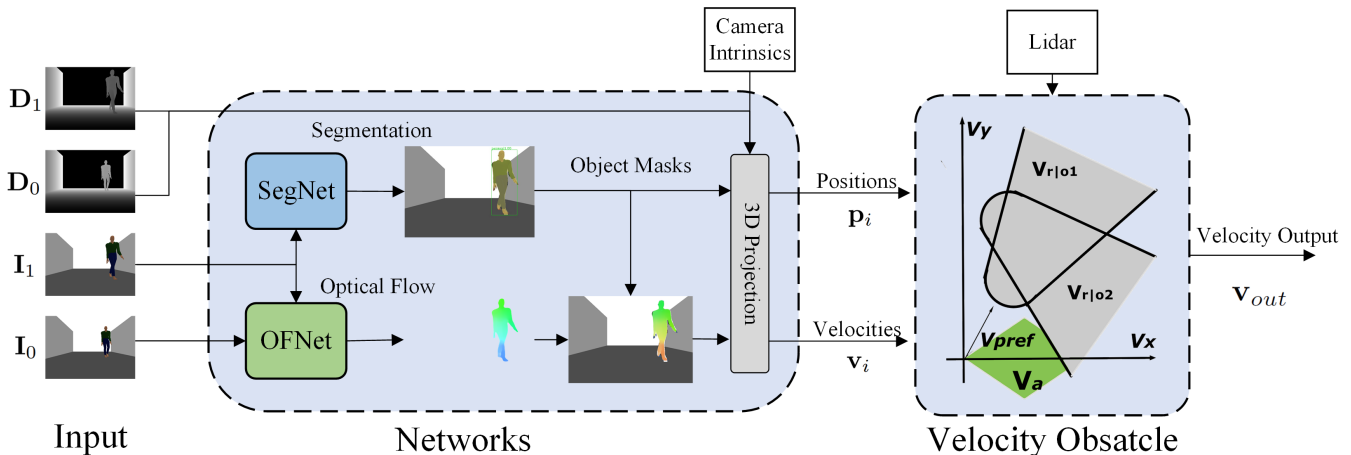


Fig. 2. OF-VO Pipeline: During each time step, our method first takes as input a pair of RGB-D images. The optical flow and segmentation masks are performed by OFNet and SegNet, respectively. Along with the depth image and intrinsic camera parameters, the 3D projection module can compute the positions and velocities from the masks and optical flow. Due to the limitation of the camera’s FOV, 2D lidar data is also collected to enhance the position estimation. Our method uses velocity obstacles to compute a collision-free velocity for the robot. Before sending control signals to the robot, a differential driving formulation is used to satisfy the dynamics constraints of the robot.

and width of the images in pixels. For simplicity, we omit t in the subscripts. $\{I_1, D_1\}$ and $\{I_0, D_0\}$ are the data collected in t_1 and t_0 respectively.

Taking $\{I_1, D_1, I_0, D_0\}$ as input, the perception networks (see in Sec. IV) can output the position $\mathbf{p}_i \in \mathbb{R}^2$ and velocity $\mathbf{v}_i \in \mathbb{R}^2$ of each obstacle i . To enhance the accuracy of camera detection and also to broaden the field of view of the robot, we use lidar to detect obstacles near the robot and fuse the data from the RGB-D camera and the 2D lidar. The perception module predicts the positions \mathbf{p}_o and velocities \mathbf{v}_o of the obstacles within its field of view (FOV).

With the dynamic information $\mathbf{p}_o, \mathbf{v}_o$ of obstacles, our method utilizes a modified VO-based algorithm to navigate the robot. Real-world scenarios inevitably have occlusions and with a limited FOV, a robot can only obtain partial observations from the environment. Different from traditional VO algorithms where the states of the obstacles are fully observable, our OF-VO is able to generate collision-free paths under partial observations. We can provide guarantees on its performance if certain assumptions are satisfied.

With unobserved objects of states $\mathbf{p}'_j, \mathbf{v}'_j$, OF-VO applies several reasonable constraints $\mathcal{C}(\mathbf{p}'_j, \mathbf{v}'_j, \mathbf{w})$ on the non-visible objects, where \mathbf{w} represents the hyper-parameters of these constraints. The partial VO algorithm can output a velocity $\mathbf{v}_{out} = VO(\mathbf{p}_o, \mathbf{v}_o, \mathbf{w})$ based on the observation. In the end, we use differential drive formulation to convert \mathbf{v}_{out} to control signals that satisfy the dynamics constraints of the robot.

Note that we divide the overall navigation into two parts, learning-based perception, and model-based collision avoidance, thereby improving the reliability and interpretability of our approach. Moreover, these two modules are strongly coupled. The hyperparameters in VO can be modified to be more conservative, which mitigates the influence of errors brought by perception. The perception part can efficiently detect and estimate the state of the obstacles, especially the ones closest to the robot. This results in reliable collision avoidance computation.

IV. PERCEPTION

The input to our perception module is a pair of consecutive RGB-D and lidar data, and the output is the estimated position \mathbf{p}_o and velocities \mathbf{v}_o of the nearby obstacles.

In our approach, we use two commodity visual sensors including Astra RGB-D camera and 2D Hokuyo Lidar. We choose to use a combination of two sensors because RGB-D camera is good at perceiving dynamic obstacles [35], while a 2D Lidar can detect the obstacles that a camera may fail to do.

A. Neural Networks

With recent progress made by deep learning in computer vision, more accurate information can be extracted from raw images with higher speed. In our method, an optical flow network and a segmentation network are used to perceive objects’ velocities and positions. The input to the neural networks are a pair of RGB-D images, and our method can compute the positions and velocities of objects appearing in the images.

At each time step, we need two consecutive frames to calculate the instantaneous velocities. Assume that the current time is t_1 and its previous time step is $t_0 < t_1$. From the RGB-D camera we have two pairs of RGB images $I_{t_1}, I_{t_0} \in \mathbb{R}^{h \times w \times 3}$ and depth images $D_{t_1}, D_{t_0} \in \mathbb{R}^{h \times w}$, where h, w is the height and width of the images in pixels. For simplicity, we omit t in the subscripts. $\{I_1, D_1\}$ and $\{I_0, D_0\}$ are the data collected in t_1 and t_0 respectively.

The input to the *OFNet* is the RGB pair I_1, I_0 , and the output is the optical flow $\mathbf{O} \in \mathbb{R}^{h \times w \times 2}$, which represents the displacement of pixels in the 2D images. Therefore, one pixel $\mathbf{p}_1 = [x_1, y_1]$ in I_1 corresponds to $\mathbf{p}_0 = [x_0, y_0] = [x_1 + \mathbf{O}(x_1, y_1, 1), y_1 + \mathbf{O}(x_1, y_1, 2)]$ in I_0 . In the depth images, \mathbf{p}_1 and \mathbf{p}_0 have the depths of $z_1 = D_1(x_1, y_1)$ and $z_0 = D_0(x_0, y_0)$. To compute the displacement of each point in the 3D world, we need to transform the pixel coordinates to camera coordinates with the help of the depth images. For a camera whose principal point is $[c_x, c_y]$ and focal lengths

are (f_x, f_y) , the 3D displacement $\mathbf{s} = [s_x, s_y, s_z] \in \mathbb{R}^{h \times w \times 3}$ from \mathbf{p}_1 to \mathbf{p}_0 can be computed by,

$$\begin{aligned} s_x &= (x_0 \cdot z_0 - c_x \cdot z_0 - x_1 \cdot z_1 + c_x \cdot z_1) / f_x, \\ s_y &= (y_0 \cdot z_0 - c_y \cdot z_0 - y_1 \cdot z_1 + c_y \cdot z_1) / f_y, \\ s_z &= z_0 - z_1. \end{aligned} \quad (1)$$

Finally, the 3D velocity of each pixel in the image \mathbf{I}_1 is given as $\mathbf{v} = \mathbf{s} / (t_0 - t_1)$. Note that $\mathbf{v} \in \mathbb{R}^{h \times w \times 3}$ is a velocity field defined on the image.

The next step is to separate objects from the raw image such that we can compute their positions and velocities. We feed image \mathbf{I}_1 to another object detection and segmentation network *SegNet* to estimate the positions and pixel-level segmentation. Assume that for the object i , *SegNet* can predict its segmentation mask $\mathbf{M}_i \in \{0, 1\}^{h \times w}$ and the position of the object in the image at $\mathbf{b}_i = [b_x, b_y]$. The depth d_i and velocity \mathbf{v}_i of an object can be calculated as the weighted mean in the masked area. For example, $d_i = (\sum \mathbf{D}_1 \odot \mathbf{M}_i) / (\sum \mathbf{M}_i)$, $\mathbf{v}_i = (\sum \mathbf{v} \odot \mathbf{M}_i) / (\sum \mathbf{M}_i)$ where \odot is the point-wise product. The 3D position of the object can be computed by $\mathbf{p}_i = [(b_x \cdot d_i - c_x \cdot d_i) / f_x, (b_y \cdot d_i - c_y \cdot d_i) / f_y, d_i]$

Compared to tracking-based velocity estimation, our method utilize pixel-level motion information. Thus, our approach does not suffer from correspondence or losing tracking target. Moreover, our *OFNet* and *SegNet* can take advantage of pre-trained models, which are trained in large volume of real-world data.

B. Sensor Fusion

Although perception by the camera has reasonable accuracy, networks are still black-boxes, and cameras usually have a relatively small field of view. In our approach, we also use 2D lidars to enhance the detection from the camera. The lidar and camera sensors are complementary, as illustrated in Figure 3. The lidar provides positions of obstacles in a wider range, while the camera can provide velocity information of the objects in front of the robot.

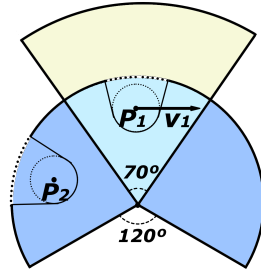


Fig. 3. The FOV of the camera and the lidar. The combination of both sensors is used to estimate the state of the obstacles and pedestrians.

Moreover, current object detection neural networks automatically neglect static obstacles (e.g. walls) by treating them as background and not segmenting them. Although the deficiency of walls usually has little influence on semantic meanings, it will hugely undermine collision avoidance and navigation. Therefore, we use lidars to detect nearby static walls. We show in our benchmarks that the RGB-D camera can predict accurate velocity and significantly improve the performance in a scene with many dynamic obstacles. The 2D lidar can also help navigation among static obstacles.

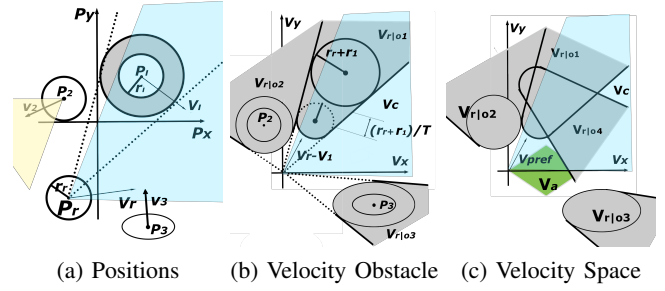


Fig. 4. Modified Velocity Obstacles algorithm with Partial Observation: These three figures illustrate our VO algorithm with partial observation. (a) shows the robot at \mathbf{p}_r , one normal obstacle at positions \mathbf{p}_1 and two obstacles out of FOV of camera at positions \mathbf{p}_2 and \mathbf{p}_3 , respectively. (b) shows the velocity obstacles in the velocity coordinates. Gray area $V_{r|o_i}$ is the forbidden area of velocities for robot(r) caused by obstacle (o_i). The blue area is one constraint for partial observation and we denote the velocity set as V_c ; (c) shows the overall velocity space of robot, where green area is the space of feasible velocities because of dynamic constraints. The gray area is the combination of VOs due to all the obstacles

V. COLLISION AVOIDANCE

With exact positions and velocities of nearby obstacles from the perception part, we use an extended Velocity-Obstacle algorithm to navigate the robot. The VO algorithm is modified due to the limited observations and non-holonomic constraints of the robot. In this section, we present our modified VO-based algorithm for partial observations and dynamic constraints.

A. VO Algorithm with Partial Observations

The VO algorithms are widely used in collision avoidance. This algorithm calculates relative positions and velocities of nearby obstacles and finds a feasible area of velocities for the robot to move. The input of our VO-based algorithm is the velocities and positions from perception modules.

Although sensors can produce information about nearby obstacles, there are still some areas out of the FOV. Intuitively, we can assume dynamic obstacles, like pedestrians, won't intentionally collide with the robot from behind. For areas inside the range of the camera, we can directly use the original VO algorithm [11]. As shown in Fig. 4(a) shows, r is the robot at position \mathbf{p}_r with velocity v_r and radius r_r . There is an obstacle at position \mathbf{p}_1 with velocity v_1 and radius r_1 . The circle with the gray area is the Minkowski Sum $s_1 \oplus -s_r$ of the robot and the obstacle. Based on the Minkowski Sum, we can view robot as a point at position \mathbf{p}_r and the obstacle has a radius of $r_r + r_1$ at position \mathbf{p}_1 . In 4(b), we assume that the velocities remain unchanged within the timestep T . Therefore, in the velocity coordinate, we can use relative velocity $\mathbf{v}_r - \mathbf{v}_1$ to calculate the feasible velocity of the robot. The gray area in the velocity coordinate is the velocity obstacle $V_{r|o}^T$ [11]. $V_{r|o}^T$ represents the forbidden area of velocities of robot r caused by obstacle o at time T . In the cone shape, the small circle at position $(\mathbf{p}_1 - \mathbf{p}_r) / T$ with radius $(r_r + r_1) / T$ is used to compute the smallest velocity that leads to collisions. The big circle defines the size of the cone shape, and it is at position $\mathbf{p}_1 - \mathbf{p}_r$ [37]. The velocity

obstacle $V_{A|B}^T$ is defined as,

$$V_{r|o}^T = \{\mathbf{v} | \exists t \in [0, T] :: t\mathbf{v} \in D(\mathbf{p}_o - \mathbf{p}_r, r_r + r_o)\} \quad (2)$$

$$D(\mathbf{p}, r) = \{\mathbf{q} | \|\mathbf{q} - \mathbf{p}\| < r\}$$

where D is the circular disk centered at position P with radius r .

Because of the limited FOV of the camera, dynamic obstacles may appear in the detection of Lidar but not of RGB-D camera, there will be a potential collision in timestep T , and it is difficult to compute velocities of such obstacles only by Lidar. In order to solve this issue, we add some velocity constraints to the original VO algorithm such that the robot won't collide even in partial observation situation. We categorize dynamic obstacles into two types, robotic obstacles with the same configurations as the robot and conscious-obstacles are pedestrians, pets or other dynamic objects.

For conscious-obstacles, as figure 4(a) shows, at the position \mathbf{p}_2 the person is walking toward the robot during the current time-step with velocity \mathbf{v}_2 . If the robot can keep enough distance between the next-step position and the person, they will never collide. Assume that the robot has a velocity $\mathbf{v}_r = (x_r, y_r)$, with a maximum of $\|\mathbf{v}_2\| = \|(x_2, y_2)\| = 1m/s$ is used in our formulation. This constraint is shown in Figure 4 (b), where robot at position \mathbf{p}_3 is under the constraint of velocity obstacle,

$$V_{r|o3}^T = \{\mathbf{v}_3 | \sqrt{\|\mathbf{v}_3 \times T\|^2} < (x_2 - x_r)^2 + (y_2 - y_r)^2\}, \quad (3)$$

where \mathbf{v}_3 is the velocity of the pedestrian.

In many cases, the obstacles have the same maximal speed as the robot. Figure 4(a) shows the relative positions and velocities, where \mathbf{p}_3 is the position of the obstacle.

For robotic dynamic obstacles, if we can keep the robot's movement within its current field of view of the camera, which is the blue cone area, robots will never collide with others, because the camera can be used to compute the velocity of obstacles. In this case, we set the constraint as Equation 4, where FOV_c is the range of the camera. In our system, $FOV_c = 70^\circ$. With this constraint, robots can only move within the FOV of the camera, and we can guarantee the robot won't collide with any obstacles with the same configuration as the robot. This constraint limits the robot's velocity in the blue cone area in Figure 4(b), and we denote the set of velocities as V_c .

$$V_c = \left\{ (v_x, v_y) \mid \left| \arctan\left(\frac{v_x}{v_y}\right) \right| < \frac{FOV_c}{2} \right\}. \quad (4)$$

If the velocity of robot satisfies $\mathbf{v}_r \notin V_{r|o}^T$, the robot r is guaranteed not to collide with the obstacle. If there are n obstacles near the robot and also with constraints for partial observation (see figure 4(c)), the feasible velocities would be given as Equation 5, where V_a is the set of velocities the robot can have because of dynamic constraints. Let $V_{r|oi}^T$ be the set of velocities out of $V_{r|o}^T$, and the final allowable

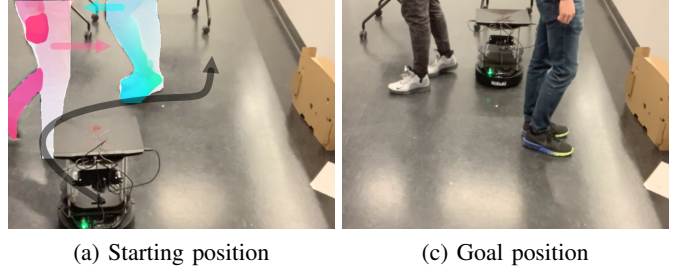


Fig. 6. Navigation across a room. Our algorithm running on Turtlebot2 can navigate the robot to avoid the pedestrians obstacles. The blue and red arrows in (a) represent the velocities estimated using the camera mounted on the robot. The black curve is the collision-free trajectory of the robot. Our robot can successfully avoid dynamic obstacles and reach the goal, as shown in (b).

velocities for the robot are given by V_r^T :

$$V_r^T = \left\{ V_c \cap V_a \cap V_{r|oi}^T \mid i \in [1, 2, \dots, n] \right\} \quad (5)$$

For each step, the robot has a preferred velocity of \mathbf{v}_{pref} according to the target position. The robot chooses a velocity $\mathbf{v}_{vo} = \arg \min_{\mathbf{v} \in V_r^T} \|\mathbf{v} - \mathbf{v}_{pref}\|_3$ from V_r^T that is nearest to \mathbf{v}_{pref} .

B. Dynamics Constraints

The output of the algorithm described above only takes into account geometric constraints. In order to use differential drive robots, we take into account non-holonomic constraints. As figure 5 shows, we use the relationships between Euler and Polar coordinates [32] to compute the velocity. Our method moves the center of the robot's configuration, \mathbf{p}_0 , to the front end of the robot, \mathbf{p}_1 , to make it fully controllable. This formulation increases the radius of the configuration to avoid collisions and makes our approach more conservative. In Equation $\mathbf{v}_{out} = (v_x, \frac{v_y}{R})$, where $\mathbf{v}_{VO} = (v_x, v_y)$, the linear and angular velocities are calculated using holonomic velocities in Euler coordinates.

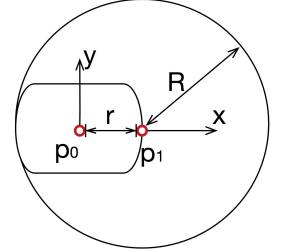


Fig. 5. Dynamics Constraints: differential drive

VI. ERROR ANALYSIS

Unlike end-to-end deep learning-based collision avoidance methods where it is hard to analyze the performance, our method explicitly uses the output of neural networks (i.e. partial observation) as intermediate results. As a result, it has better interpretability. We can analyze the estimation errors and provide a certain level of guarantee with our approach.

As reported by FlowNet2 [19], their average endpoint error in KITTI 2012 is $e_f = 4.09$, which means that their predicted optical flow is an average of 4.09 pixels away from the ground truth. In the perception part, we use two networks Mask-RCNN and FlowNet2, to estimate segmentation and optical flow, respectively. According to Equation 1, for an object whose depth is z , an error of e_f pixels in optical

flow would bring an error of $e_f \cdot z / (f \cdot \Delta t)$ to its velocity estimation. In our implementation, we have $f_x = f_y = 457$, time interval $\Delta = 0.2$, so the error for an object at $0.5m$ away would be $0.025m/s$.

The error of *SegNet* is harder to quantify. From Figure 1, we can see that the segmentation of the pedestrian is reasonably good in our scene. The average precision (.50 IoU) of Mask-RCNN is 62.3% [15] on the COCO dataset [22], which means nearly two-thirds of predictions have more than .50 IoU. In order to make our collision avoidance more conservative, we enlarge the bounding box of moving obstacles by more than 50%. In our experiments where the speed of pedestrians is 1 m/s, the average absolute error is $0.076m$ for position estimation and $0.11m/s$ for velocity estimation. This error is tolerable in benchmarks when we use a slightly larger bounding box for the robot and obstacles. To make our method even more robust, Lidar is used to detect the distance from the surrounding obstacles. As a result, the robot is aware of nearby objects even when the camera-based detection fails.

VII. RESULTS

In this section, we highlight the implementation details. We also compare performances using different sensors and show the improvement of the performance of our approach in scenarios with partial observation. Finally, we compare our method with other traditional (DWA) [12] and deep reinforcement learning (DRL) [9] methods.

A. Experimental Setup

We generated results on a laptop with an Intel i7-9750H CPU (2.6 GHz) with 32 GB memory and an Nvidia GeForce RTX 2070 GPU. We use Turtlebot2 as the robot platform to implement our method P-VO. Astra RGB-D camera and Hokuyo Lidar. The resolution of the RGB-D camera is 640×480 , and 520 range data for Lidar. We run our system with Ubuntu 18.04, ROS Melodic, Gazebo 9.0.0, and PyTorch 1.4. The segmentation network is mask-RCNN from detectron2 [41] and optical flow network is FlowNet2 [19]. Figure 6 shows a Turtlebot2 with our algorithm moving across a room. Inside the room are static obstacles as well as pedestrians. Our method can successfully drive the robot from the start point to the target while avoiding collisions.

Success Rate	Lidar+RGB-D	RGB-D	Lidar
Empty	100%	100%	100%
Static Obstacles	100%	5%	100%
Dynamic Obstacles	92%	85%	30%
Complex Obstacles	91%	64%	41%

TABLE II. Success rate using different sensors. Our sensor fusion of RGB-D and lidar achieves higher success rate than only using an RGB-D camera or a Lidar. RGB-D camera can enhance the velocity estimation of dynamic objects, while the lidar helps to avoid static obstacles.

B. Scenarios Used for Testing

In order to test the performance of our method detailed in the improvement of using different sub-models of the

method, we created different scenarios. Here are five scenarios as in Figure 7.

1. **Empty** (Figure 7(a)): In this scenario, OF-VO tested with random goal and start position. It is used to test if the robot has the basic functionality to go to the goal position.
2. **Static** (Figure 7(b)): This scenarios is for robot to go around static obstacles and go to the goal position.
3. **Dynamic** (Figure 7(c)): In this scenario, there is a crowd of people moving towards the robot from the front. The robot needs to avoid pedestrians and find its way to the goal position.
4. **Complex** (Figure 7(d)): In this scenario there are not only static but also dynamic obstacles. A robot is required to have the ability to avoid both types of obstacles.
5. **Cross** (Figure 7(e)): In this scenario, people are moving from side of the robot. This scenario requires the ability to avoid dynamic obstacles from both sides and challenging in terms of perception issues.

C. Ablation Study on Sensors

We conduct an ablation study of the sensor choices in Table II. We run testing experiments to get the success rate of each model. In four sorts of scenarios Figure 7(a to d).

The results are shown in Table II. In empty scenarios, all those three models work well and go towards the goal smoothly, as shown in Figure 7(a). In the scenario with only big static obstacles (Figure 7(b)), the robot with only the RGB-D camera can barely go through the maze. The reason is that the segmentation neural network would neglect walls as background, instead of treating it as an obstacle. Compared with the camera, the lidar has the advantage to detect static obstacles.

In the scene with only dynamic obstacles (Figure 7(c)), our perception module can successfully extract the velocities of pedestrians and prominently outperforms Lidar-only robot shown in the third row of Table II, which cannot obtain the obstacle velocities.

In the fourth row of Table II, there are mixed obstacles corresponding to moving pedestrians and static walls, shown in Figure 7(d). Because Lidar has a big field of view and high accuracy in terms of distance detection, it is used to enhance the position detection to dynamic obstacles by using depth images. As a result, our sensor fusion of RGB-D and lidar achieves much higher success rate than either RGBD-only or Lidar-only perception.

D. Partial-Observation Based VO

In our approach, because of the limitation of sensors, we have only partial observation around the robot. We present a VO-based method with a different formulation. In order to compare the performance of our method with the original VO method, which doesn't consider partial observation, we tested OF-VO in scenarios with pedestrians going across from outside of the view of the camera, as shown in Figure 7(e).

The successful rate using our approach is 89%. However, without the constraints, the rate of successes drop to around

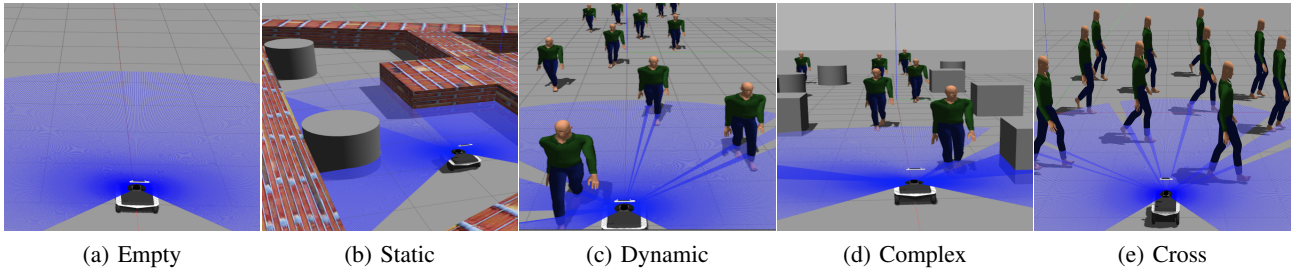


Fig. 7. Simulation Scenarios: We use five scenes to run the comparison and ablation study. The scenes corresponding to (c), (d) and (er) are dynamic scenes with multiple pedestrians. The robot goes from a start point to a goal point, while avoiding dynamic and static obstacles.

60%. Our method improves by $\frac{1}{3}$ in the dynamic scenes, where pedestrians may walk towards the robot from outside the field-of-view of the camera.

E. Performance: Local Navigation

We compare our algorithm (OF-VO) with two other collision avoidance methods, Dynamic-Window Approach (DWA) and another Deep Reinforcement Learning-based (DRL) approach[9]. We compare these three algorithms using three criteria:

Trajectory Length: This value gives information about the accuracy of each algorithm, the shortest length has better accuracy in terms of calculation of the path and perception.

Navigation Time: The value shows how long each method takes to navigate the robot towards the goal. It gives information about the processing speed and also the timestep used for navigation.

Success Rate: This value shows the overall performance in terms of collision avoidance and safety.

Results in Figure VII-D indicate that our method outperforms the other two algorithms in terms of trajectory length, navigation time, and success rate. Our method (OF-VO) can reach the goal in the shortest distance and time because that our model-based VO can find a path to the target without redundant oscillations or freezing. This highlights the reliability of our approach

As the table shows, in empty scenarios, all the models of DRL, DWA and OF-VO have good performance in terms of reaching the goal. Since DWA is better in terms of velocity optimization with control of acceleration, the trajectory of DWA is the shortest. However, our OF-VO is the fastest approach. For scenarios containing both static and dynamic obstacles, our method outperforms the two methods in terms of three factors. The table also shows that DWA has less stability in scenarios with dynamic obstacles. In these scenarios, if an obstacle runs across the robot from its side, DWA cannot avoid the collisions. This highlights the improved performance and reliability of OF-VO.

VIII. CONCLUSIONS, LIMITATIONS, AND FUTURE WORK

In this paper, we present a hybrid navigation algorithm that combines learning-based perception and model-based collision avoidance. We have implemented OF-VO on a Turtlebot with commodity visual sensors, including an RGB-D camera and a lidar. We have evaluated the performance

in complex dynamic scenes with multiple pedestrians and highlight the benefits over prior model-based (DWA) and learning-based (DRL) methods in terms of success rate and reliability.

Although our method performs well in general, it has some limitations. In particular, the Velocity-Obstacle is a local navigation method and the robot is constrained not to move in a backward manner or backtrack. As a result, the robot may get stuck in an impasse where there is no feasible velocity (i.e. freezing behavior). Moreover, the optical flow estimation has lower performance for large displacements. Moreover, if there are fast-moving obstacles outside the field-of-view of the camera, they can result in collisions. As part of future work, we would like to overcome these limitations and also combine with global navigation methods. We would like to evaluate the performance of different robots in outdoor scenes.

REFERENCES

- [1] Andrej Babinec, František Duchoň, Martin Dekan, Peter Pászto, and Michal Kelemen. Vfh* tdt (vfh* with time dependent tree): A new laser rangefinder based obstacle avoidance method designed for environment with non-static obstacles. *Robotics and autonomous systems*, 62(8):1098–1115, 2014.
- [2] H. Bai, S. Cai, N. Ye, D. Hsu, and W. S. Lee. Intention-aware online pomdp planning for autonomous driving in a crowd. In *2015 IEEE International Conference on Robotics and Automation (ICRA)*, pages 454–460, May 2015.
- [3] Daman Bareiss and Jur Van den Berg. Reciprocal collision avoidance for robots with linear dynamics using lqr-obstacles. In *2013 IEEE International Conference on Robotics and Automation*, pages 3847–3853. IEEE, 2013.
- [4] Osbert Bastani, Yewen Pu, and Armando Solar-Lezama. Verifiable reinforcement learning via policy extraction. In *Advances in Neural Information Processing Systems 31*, pages 2494–2504. Curran Associates, Inc., 2018.
- [5] Thomas Brox, Andrés Bruhn, Nils Papenberg, and Joachim Weickert. High accuracy optical flow estimation based on a theory for warping. In *European conference on computer vision*, pages 25–36. Springer, 2004.
- [6] Haiyang Chao, Yu Gu, and Marcello Napolitano. A survey of optical flow techniques for robotics navigation applications. *Journal of Intelligent & Robotic Systems*, 73(1-4):361–372, 2014.
- [7] Alexey Dosovitskiy, Philipp Fischer, Eddy Ilg, Philip Hausser, Caner Hazirbas, Vladimir Golkov, Patrick Van Der Smagt, Daniel Cremers, and Thomas Brox. FlowNet: Learning optical flow with convolutional networks. In *Proceedings of the IEEE international conference on computer vision*, pages 2758–2766, 2015.
- [8] Michael Everett, Yu Fan Chen, and Jonathan P How. Motion planning among dynamic, decision-making agents with deep reinforcement learning. In *IROS*, pages 3052–3059. IEEE, 2018.
- [9] Tingxiang Fan, Pinxin Long, Wenxi Liu, and Jia Pan. Fully distributed multi-robot collision avoidance via deep reinforcement learning for safe and efficient navigation in complex scenarios. *arXiv preprint arXiv:1808.03841*, 2018.

Scenarios	Trajectory length (m)			Navigation Time (sec)			Success Rate (%)		
	OF-VO	DWA	DRL	OF-VO	DWA	DRL	OF-VO	DWA	DRL
Empty	5.95	5.80	6.05	5.9	14.6	24.9	100	100	100
Static obstacles	8.50	18.16	9.9	10.2	15.6	19.11	100	95	90
Dynamic obstacles	21.27	29.98	42.19	26.6	42.93	43.6	92	20	55

TABLE III. Quantitative comparison with other collision avoidance methods. The table compares OF-VO with DWA [12] and DRL methods [9] in terms of accuracy (trajectory length: lower is better), speed (navigation time: lower is better) and reliability (success rate: higher is better). Our method, OF-VO, outperforms other methods in all these scenarios. With the complexity of environment increasing, our method exhibits better performance than the other two. DWA has the shortest length in empty scenario, because it takes into consideration accelerations. Our method achieves much higher success rate in dynamic scenes and is more reliable. This highlights the benefits of our hybrid approach.

- [10] Tingxiang Fan, Pinxin Long, Wenxi Liu, Jia Pan, Ruigang Yang, and Dinesh Manocha. Learning resilient behaviors for navigation under uncertainty environments. *arXiv preprint arXiv:1910.09998*, 2019.
- [11] Paolo Fiorini and Zvi Shiller. Motion planning in dynamic environments using velocity obstacles. *The International Journal of Robotics Research*, 17(7):760–772, 1998.
- [12] Dieter Fox, Wolfram Burgard, and Sebastian Thrun. The dynamic window approach to collision avoidance. *IEEE Robotics & Automation Magazine*, 4(1):23–33, 1997.
- [13] Ross Girshick, Jeff Donahue, Trevor Darrell, and Jitendra Malik. Rich feature hierarchies for accurate object detection and semantic segmentation. In *Computer Vision and Pattern Recognition*, 2014.
- [14] B. Gopalakrishnan, A. K. Singh, M. Kaushik, K. M. Krishna, and D. Manocha. Prvo: Probabilistic reciprocal velocity obstacle for multi robot navigation under uncertainty. In *2017 IEEE/RSJ International Conference on Intelligent Robots and Systems (IROS)*, pages 1089–1096, Sep. 2017.
- [15] Kaiming He, Georgia Gkioxari, Piotr Dollár, and Ross Girshick. Mask r-cnn. In *Proceedings of the IEEE international conference on computer vision*, pages 2961–2969, 2017.
- [16] Daniel Hennes, Daniel Claes, Wim Meeussen, and Karl Tuyls. Multi-robot collision avoidance with localization uncertainty. In *AAMAS*, pages 147–154, 2012.
- [17] Roberto Henschel, Laura Leal-Taixé, Daniel Cremers, and Bodo Rosenhahn. Fusion of head and full-body detectors for multi-object tracking. In *Proceedings of the IEEE Conference on Computer Vision and Pattern Recognition Workshops*, pages 1428–1437, 2018.
- [18] Berthold KP Horn and Brian G Schunck. Determining optical flow. In *Techniques and Applications of Image Understanding*, volume 281, pages 319–331. International Society for Optics and Photonics, 1981.
- [19] Eddy Ilg, Nikolaus Mayer, Tommo Saikia, Margret Keuper, Alexey Dosovitskiy, and Thomas Brox. FlowNet 2.0: Evolution of optical flow estimation with deep networks. In *Proceedings of the IEEE conference on computer vision and pattern recognition*, pages 2462–2470, 2017.
- [20] Amichai Levy, Chris Keitel, Sam Engel, and James McLurkin. The extended velocity obstacle and applying orca in the real world. In *2015 IEEE International Conference on Robotics and Automation (ICRA)*, pages 16–22. IEEE, 2015.
- [21] Mingming Li, Rui Jiang, Shuzhi Sam Ge, and Tong Heng Lee. Role playing learning for socially concomitant mobile robot navigation. *CAA Transactions on Intelligence Technology*, 3(1):49–58, 2018.
- [22] Tsung-Yi Lin, Michael Maire, Serge Belongie, James Hays, Pietro Perona, Deva Ramanan, Piotr Dollár, and C Lawrence Zitnick. Microsoft coco: Common objects in context. In *European conference on computer vision*, pages 740–755. Springer, 2014.
- [23] Anton Milan, Stefan Roth, and Konrad Schindler. Continuous energy minimization for multitarget tracking. *IEEE transactions on pattern analysis and machine intelligence*, 36(1):58–72, 2013.
- [24] Volodymyr Mnih, Adria Puigdomenech Badia, Mehdi Mirza, Alex Graves, Timothy Lillicrap, Tim Harley, David Silver, and Koray Kavukcuoglu. Asynchronous methods for deep reinforcement learning. In *International conference on machine learning*, pages 1928–1937, 2016.
- [25] Mark Pfeiffer, Michael Schaeuble, Juan Nieto, Roland Siegwart, and Cesar Cadena. From Perception to Decision: A Data-driven Approach to End-to-end Motion Planning for Autonomous Ground Robots. *arXiv e-prints*, page arXiv:1609.07910, Sep 2016.
- [26] Joseph Redmon, Santosh Divvala, Ross Girshick, and Ali Farhadi. You only look once: Unified, real-time object detection. In *Proceedings of the IEEE conference on computer vision and pattern recognition*, pages 779–788, 2016.
- [27] Joseph Redmon and Ali Farhadi. Yolo9000: better, faster, stronger. In *Proceedings of the IEEE conference on computer vision and pattern recognition*, pages 7263–7271, 2017.
- [28] Shaoqing Ren, Kaiming He, Ross Girshick, and Jian Sun. Faster R-CNN: Towards real-time object detection with region proposal networks. In *Advances in Neural Information Processing Systems (NIPS)*, 2015.
- [29] Adarsh Jagan Sathyamoorthy, Jing Liang, Utsav Patel, Tianrui Guan, Rohan Chandra, and Dinesh Manocha. Densecaavoid: Real-time navigation in dense crowds using anticipatory behaviors. *arXiv preprint arXiv:2002.03038*, 2020.
- [30] John Schulman, Filip Wolski, Prafulla Dhariwal, Alec Radford, and Oleg Klimov. Proximal policy optimization algorithms. *arXiv preprint arXiv:1707.06347*, 2017.
- [31] Shingo Shimoda, Yoji Kuroda, and Karl Iagnemma. Potential field navigation of high speed unmanned ground vehicles on uneven terrain. In *Proceedings of the 2005 IEEE International Conference on Robotics and Automation*, pages 2828–2833. IEEE, 2005.
- [32] Jamie Snape, Jur Van Den Berg, Stephen J Guy, and Dinesh Manocha. Smooth and collision-free navigation for multiple robots under differential-drive constraints. In *2010 IEEE/RSJ International Conference on Intelligent Robots and Systems*, pages 4584–4589. IEEE, 2010.
- [33] Deqing Sun, Xiaodong Yang, Ming-Yu Liu, and Jan Kautz. Models matter, so does training: An empirical study of cnns for optical flow estimation. *arXiv preprint arXiv:1809.05571*, 2018.
- [34] L. Tai, J. Zhang, M. Liu, and W. Burgard. Socially compliant navigation through raw depth inputs with generative adversarial imitation learning. In *ICRA*, pages 1111–1117, May 2018.
- [35] Lei Tai, Jingwei Zhang, Ming Liu, and Wolfram Burgard. Socially compliant navigation through raw depth inputs with generative adversarial imitation learning. In *2018 IEEE International Conference on Robotics and Automation (ICRA)*, pages 1111–1117. IEEE, 2018.
- [36] V Tchernykh, M Beck, and K Janschek. Optical flow navigation for an outdoor uav using a wide angle mono camera and dem matching. *IFAC Proceedings Volumes*, 39(16):590–595, 2006.
- [37] Jur Van Den Berg, Stephen J Guy, Ming Lin, and Dinesh Manocha. Reciprocal n-body collision avoidance. In *Robotics research*, pages 3–19. Springer, 2011.
- [38] Jur Van Den Berg, Jamie Snape, Stephen J Guy, and Dinesh Manocha. Reciprocal collision avoidance with acceleration-velocity obstacles. In *2011 IEEE International Conference on Robotics and Automation*, pages 3475–3482. IEEE, 2011.
- [39] Jur Van Den Berg, David Wilkie, Stephen J Guy, Marc Niethammer, and Dinesh Manocha. Lqg-obstacles: Feedback control with collision avoidance for mobile robots with motion and sensing uncertainty. In *2012 IEEE International Conference on Robotics and Automation*, pages 346–353. IEEE, 2012.
- [40] David Wilkie, Jur Van Den Berg, and Dinesh Manocha. Generalized velocity obstacles. In *2009 IEEE/RSJ International Conference on Intelligent Robots and Systems*, pages 5573–5578. IEEE, 2009.
- [41] Yuxin Wu, Alexander Kirillov, Francisco Massa, Wan-Yen Lo, and Ross Girshick. Detectron2. <https://github.com/facebookresearch/detectron2>, 2019.
- [42] Linhai Xie, Sen Wang, Andrew Markham, and Niki Trigoni. Towards Monocular Vision based Obstacle Avoidance through Deep Reinforcement Learning. *arXiv e-prints*, page arXiv:1706.09829, Jun 2017.
- [43] Jingwei Zhang, Jost Tobias Springenberg, Joschka Boedecker, and Wolfram Burgard. Deep reinforcement learning with successor features for navigation across similar environments. In *2017 IEEE/RSJ International Conference on Intelligent Robots and Systems (IROS)*, pages 2371–2378. IEEE, 2017.
- [44] Yuke Zhu, Roozbeh Mottaghi, Eric Kolve, Joseph J. Lim, Abhinav Gupta, Li Fei-Fei, and Ali Farhadi. Target-driven Visual Navigation in Indoor Scenes using Deep Reinforcement Learning. *arXiv e-prints*,

page arXiv:1609.05143, Sep 2016.

- [45] Simon Zingg, Davide Scaramuzza, Stephan Weiss, and Roland Siegwart. Mav navigation through indoor corridors using optical flow. In *2010 IEEE International Conference on Robotics and Automation*, pages 3361–3368. IEEE, 2010.